Inorganic Chemistry
Article
pubs.acs.org/IC

$A_2MnU_3O_{11}$ (A = K, Rb) and $Li_{3.2}Mn_{1.8}U_6O_{22}$: Three New Alkali-Metal Manganese Uranium(VI) Oxides Related to Natrotantite

Cory Michael Read, Gregory Morrison, Jeongho Yeon, Mark D. Smith, and Hans-Conrad zur Loye*

Department of Chemistry and Biochemistry, University of South Carolina, Columbia, South Carolina 29208, United States

Supporting Information

ABSTRACT: Single crystals of three new alkali-metal manganese uranium oxides, $K_2MnU_3O_{11}$, $Rb_2MnU_3O_{11}$, and $Li_{3.2}Mn_{1.8}U_6O_{22}$, have been grown from molten chloride fluxes and structurally characterized by single-crystal X-ray diffraction. The first two compounds crystallize in the trigonal space group, $R\bar{3}c$, in the three-dimensional (3D), natrotantite structure composed of α-U_3O_8-topological layers connected via MnO_6 octahedra. The Li-containing compound crystallizes in the monoclinic space group, *Cc*, with a related 3D structure, composed of β-U_3O_8-topological sheets connected via irregular MnO_7 polyhedra. All three compounds exhibit typical uranyl, UO_2^{2+}, coordination environments consisting of either UO_7 pentagonal bipyramids or UO_6 flattened octahedra. The lattice parameters of the new oxides are $K_2MnU_3O_{11}$, $a = 6.8280(2)$ Å, $c = 36.8354(17)$ Å; $Rb_2MnU_3O_{11}$, $a = 6.8407(2)$ Å, $c = 37.5520(17)$ Å; and $Li_{3.2}Mn_{1.8}U_6O_{22}$, $a = 11.8958(8)$ Å, $b = 10.9639(7)$ Å, $c = 13.3269(8)$ Å, and $\beta = 91.442(4)°$. The magnetic susceptibilities of the K and Rb phases are discussed.

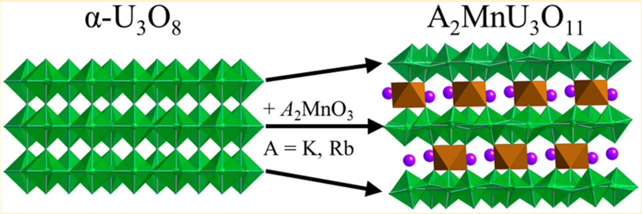

INTRODUCTION

The investigation of uranium-containing oxide compositions continues to be of interest due to the need for new materials and improved chemical understanding of uranium-containing materials for long-term nuclear waste storage applications as well as for new fuel rod technologies. The crystal growth of novel compositions is essential to improve our understanding of this vast class of materials, where thorough structural characterizations are essential for understanding their observed properties. Various synthetic approaches have been applied to grow single crystals of complex uranium-containing oxides including chemical vapor transport,[1−5] hydrothermal,[6−10] subcritical hydrothermal,[11−17] solid state processing,[18−29] and flux growth.[30−36]

The flux growth method is a widely applied method for exploratory crystal growth[37] and has proven to be an effective approach for the growth of uranium-containing oxides. Alkali-metal hydroxides and carbonate fluxes have been used in the synthesis of mostly alkali-metal/alkaline-earth uranium oxides or uranium tungstates, molybdates, or niobates.[30−36] Recently, halide fluxes have been utilized to promote the formation of previously reported oxides for which, however, no published single crystal data were available[38] as well as for altogether novel compositions.[39−42] Most of the compounds that have been synthesized this way contain first-row transition metals in addition to the uranium, which led us to further utilize these fluxes for exploratory crystal growth of complex uranium oxides containing 3d transition metals.

The most common structural feature of uranium(VI)-containing oxides is the linear or nearly linear uranyl ion, UO_2^{2+}. The uranyl ion loosely coordinates four, five, or six additional oxygen atoms in the equatorial region, forming square-, pentagonal-, or hexagonal-bipyramids. The axial, uranyl oxygen atoms are most often terminal, leading to the formation of predominantly zero-, one-, and two-dimensional (0D, 1D, and 2D, respectively) structures. Three-dimensional (3D) structures are less common; however, they often exhibit unique framework topologies.[43]

The structure of natrotantite, $Na_2Ta_4O_{11}$, is composed of α-U_3O_8-type sheets of edge-sharing TaO_7 pentagonal bipyramids (P-layers) connected via TaO_6 octahedra (O-layers). This 3D structural family is quite versatile, exhibiting several different stacking sequences. The reported phases in this class have all been tantalates or niobates, having TaO_7 or NbO_7 polyhedral sheets, respectively. The respective connecting layers are typically TaO_6 or NbO_6 octahedra along with an electropositive cation. This class has been generalized as $A_xTa_{3n+1}O_{8n+3}$,[44] where A is a monovalent (Na, Cu, Ag),[44−46] divalent (Ca, Sr, Pb),[44,47,48] or trivalent (lanthanides, Bi) cation,[44,49] where Ta can be substituted by Nb,[50−52] and where n is equal to 1 or 2. The value of n corresponds to the thickness of the U_3O_8-type stack, where $n = 1$ represents a stacking sequence of PO and $n = 2$ represents a PPO sequence. Noninteger values are possible for n, for example, $n = 1.5$ in $Cu_5Ta_{11}O_{30}$,[45] which has a stacking order of POPPO. Some additional versatility can be imposed on the structure by substituting a different metal cation for Ta into the O-layer, as is the case with $M_2Ta_6O_{19}$ (M = Th, U)[53] and $M_4Ta_{18}O_{53}$ (M = Th, U),[3] with respective stacking sequences of PPO and PPPO. To date, there have been no reported cases where the P-layer is composed of UO_7 pentagonal bipyramids.

Received: May 5, 2015
Published: July 9, 2015

DOI: 10.1021/acs.inorgchem.5b01004
Inorg. Chem. 2015, 54, 6993−6999

The crystal growth and structural characterization of two novel quaternary uranium oxides exhibiting the natrotantite-type, $K_2MnU_3O_{11}$ (**1**), $Rb_2MnU_3O_{11}$ (**2**), and a natrotantite-related structure, $Li_{3.2}Mn_{1.8}U_6O_{22}$ (**3**), are presented herein. The optical properties and temperature dependence of the magnetic susceptibilities are reported for **1** and **2**.

■ EXPERIMENTAL SECTION

Reagents. U_3O_8 (International Bioanalitics Industries Inc., ACS grade), $MnCl_2{\cdot}4H_2O$ (Alfa Aesar, 99%), LiCl (Acros, 99.9%), KCl (Mallinckrodt, ACS grade), and RbCl (Alfa Aesar, 99%) were used as received. **Caution!** *Although the uranium precursors used contain depleted uranium, standard safety measures for handling radioactive substance should be followed.*

Synthesis. Single crystals of the title materials were grown from molten chloride fluxes where the precise crystal growth conditions were optimized for each composition to maximize yield and crystal quality.

For the preparation of $K_2MnU_3O_{11}$ (**1**), 0.33 mmol U_3O_8, 2 mmol $MnCl_2{\cdot}4H_2O$, and 20 mmol KCl were added to an alumina crucible (18 mm D × 26 mm H, 5 mL) that was uncovered. The reactants were heated at a rate of 10 °C/min to 900 °C, held there for 12 h, and cooled to room temperature by turning off the furnace. The majority of the flux had evaporated throughout the course of the reaction. The reaction yielded approximately 90% large plate-like crystals of **1** along with some black, polycrystalline material, which could not be identified. An optical image of the crystals of **1** are presented in Figure 1a.

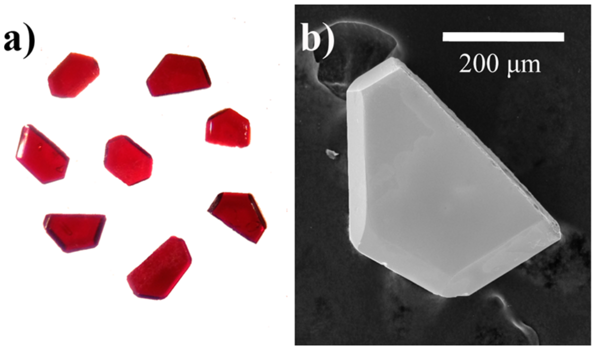

Figure 1. Optical (a) and SEM (b) images of $K_2MnU_3O_{11}$ crystals.

The rubidium analogue, $Rb_2MnU_3O_{11}$ (**2**), formed in approximately 70% yield when RbCl was used as the flux. The reaction was covered with an alumina disc that rested loosely on top of the crucible and heated at a rate of 20 °C/min to 950 °C, allowed to dwell for 12 h, and cooled to room temperature by turning off the furnace. The majority of the flux had evaporated throughout the course of the reaction, which yielded plate-like crystals of **2** along with some yellow $Rb_2U_2O_7$ that grew on the surface of some of the title crystals and some black, polycrystalline material, which could not be identified.

For the preparation of $Li_{3.2}Mn_{1.8}U_6O_{22}$ (**3**), 1 mmol U_3O_8, 1.5 mmol $MnCl_2{\cdot}4H_2O$, and 40 mmol LiCl were added to an alumina crucible and covered with an alumina disc. The charge was heated to 900 °C at a rate of 10 °C/min, allowed to dwell for 12 h, cooled to 500 °C at a rate of 0.1 °C/min, and finally cooled to room temperature by turning off the furnace.

The flux remaining after each reaction was washed away with water, aided by sonication, and the crystals were isolated by vacuum filtration. The large red–orange plate-like crystals of **1** and **2** were easily separated from the heterogeneous mixture by use of a 355 μm sieve. A pure sample large enough for property measurements could not be obtained for **3**, as the crystals were visually indistinguishable from crystals of Mn_3O_4, which was identified as a byproduct.

Single-Crystal X-ray Diffraction. X-ray intensity data from plate-like crystals of **1**, **2**, and **3** were collected at 296(2) K using a Bruker SMART APEX diffractometer (Mo Kα radiation, λ = 0.71073 Å).[54] The data collection covered 99.8–100% of reciprocal space to $2\theta_{max}$ = 64.0–75.6°, with R_{int} = 0.0461–0.0662 after absorption correction. The raw area detector data frames were reduced and corrected for absorption effects with the SAINT+ and SADABS programs.[54] Final unit cell parameters were determined by least-squares refinements of 2391–5129 reflections from the data sets. Direct methods structure solution, difference Fourier calculations, and full-matrix least-squares refinement against F^2 were performed with SHELXS/L[55] or with SHELXL-2013/4[55] using the ShelXle interface.[56] Crystallographic data for the title compounds can be found in Table 1.

Table 1. Crystallographic Data for $K_2MnU_3O_{11}$, $Rb_2MnU_3O_{11}$, and $Li_{3.2}Mn_{1.8}U_6O_{22}$

empirical formula	$K_2MnU_3O_{11}$	$Rb_2MnU_3O_{11}$	$Li_{3.2}Mn_{1.8}U_6O_{22}$
formula weight (amu)	1023.23	1115.97	1902.08
crystal system	trigonal	trigonal	monoclinic
space group	$R\bar{3}c$	$R\bar{3}c$	Cc
a (Å)	6.8280(2)	6.8407(2)	11.8958(8)
b (Å)	6.8280(2)	6.8407(2)	10.9639(7)
c (Å)	36.8354(17)	37.5520(17)	13.3269(8)
β (deg)	90	90	91.442(2)
volume (Å^3)	1487.25(9)	1521.82(9)	1737.60(19)
Z	6	6	4
ρ_{calc} (g/cm^3)	6.855	7.306	7.271
μ (mm^{-1})	50.985	58.539	57.092
temperature (K)	296(2)	296(2)	296(2)
wavelength (Å)	0.71073	0.71073	0.71073
final R indexes [$I \geq 2\sigma(I)$]	R_1 = 0.0188, wR_2 = 0.0444	R_1 = 0.0227, wR_2 = 0.0481	R_1 = 0.0473, wR_2 = 0.0900
final R indexes [all data]	R_1 = 0.0195, wR_2 = 0.0447	R_1 = 0.0252, wR_2 = 0.0488	R_1 = 0.0573, wR_2 = 0.0936

For **1** and **2**, all atoms were refined with anisotropic displacement parameters. Trial refinements of the site occupancy factors (*sofs*) of the metal atoms showed no significant deviations from full occupancy. The reported atomic coordinates were standardized with Structure Tidy program.[57]

For **3**, the pattern of systematic absences in the intensity data was consistent with the space groups *Cc* and *C*2/*c*. Intensity statistics suggested an acentric structure. A reasonable solution was obtained in the acentric group *Cc*. Checking of the finished structure with the ADDSYM program in PLATON found no missed symmetry elements.[58] An ADDSYM check using only the fully ordered uranium and oxygen atom positions gave the same result. Trial refinements of the *sofs* of the uranium atoms showed no significant deviations from full occupancy. A model invoking Mn/Li mixing on these four sites generates the reported composition of $Li_{3.18}Mn_{1.82}U_6O_{22}$, with an average Mn oxidation state of +2.65. Each site was constrained to full occupancy by the Mn/Li mixture. This model is certainly reasonable, especially considering the formation of the mixed-valent compound Mn_3O_4 (average Mn oxidation state +2.67) in the same reaction vessel. The lithium site (Li5) was located after all other metal and oxygen atom sites were identified. We believe the structural model presented herein is the best interpretation of the diffraction data from a nonideal, disordered crystal. Because of the weak scattering power of lithium, especially amidst uranium atoms, and the imposition of full occupancy on the mixed Li/Mn sites, the composition likely has a larger uncertainty than that calculated from the refined occupancies.

Powder X-ray Diffraction. Powder X-ray diffraction data were collected for **1** and **2** on a Rigaku D/Max-2100 powder X-ray diffractometer using Cu Kα radiation. The step-scan covered the angular range 5–70° 2θ in steps of 0.04°. The calculated and experimental PXRD patterns are in excellent agreement (see Figures S1 and S2).

Energy-Dispersive Spectroscopy (EDS). Elemental analysis was performed on the flux-grown crystals using a TESCAN Vega-3 SBU scanning electron microscope (SEM) with EDS capabilities. The crystals were mounted on carbon tape and analyzed using a 20 kV accelerating voltage and an accumulation time of 20 s. As a qualitative measure, the EDS confirmed the presence of each heavy element in the title compounds. Final elemental compositions, including the presence and concentration of the light elements Li and O, were determined by structure solution. An SEM image of a $K_2MnU_3O_{11}$ is presented in Figure 1b.

Optical Spectroscopy. UV−vis diffuse reflectance spectra of polycrystalline powder samples of the reported materials were obtained using a PerkinElmer Lambda 35 UV/vis scanning spectrophotometer equipped with an integrating sphere in the range 200−900 nm. Because uranyl compounds can exhibit luminescence, spectra of polycrystalline powder samples of **1** and **2** were obtained using a PerkinElmer LS-55 fluorescence spectrometer. Excitation and emission scans were performed in the 250−450 and 450−900 nm ranges, respectively. No luminescence was observed.

Magnetic Property Measurement. Magnetic properties of $A_2MnU_3O_{11}$ (A = K, Rb) were measured on a Quantum Design magnetic property measurement system (QD MPMS 3). Ground samples weighing ∼25 mg were loaded into VSM powder holders and massed on a balance sensitive to 0.01 mg. Magnetic susceptibilities were measured as a function of temperature under zero-field-cooled conditions from 2 to 300 K at an applied field of 1000 Oe. The raw moments were corrected for sample shape and radial offset effects using a combination of DC scan and VSM scan data collected at 2 K.[59]

■ RESULTS AND DISCUSSION

Synthesis. Flux crystal growth has been a very successful approach for exploratory synthesis of quaternary oxides.[37] The alkali-metal chloride fluxes have been used to synthesize several uranium-containing oxides.[38−40,60,61] At the reaction temperatures reported herein, the chloride fluxes used completely dissolved the starting materials; however, an excess of $MnCl_2 \cdot 4H_2O$ was needed to form the products due to vapor transport of the Mn in the chloride-rich environment. For **1**−**3**, the majority of the flux had evaporated throughout the course of the reaction; however, **2** and **3** required slower evaporation of the flux, which was achieved by loosely covering the crucibles with alumina discs. By controlling the degree of saturation of the solution through evaporation of the flux, it is possible to grow the title compounds with good yields. Slow cooling alone results in smaller crystals and much lower yields of the title compounds, and for **3**, in the absence of using a crucible cover, the reactions produced only simple ternary lithium uranium(VI) oxides.

Structures. $K_2MnU_3O_{11}$ (**1**) and $Rb_2MnU_3O_{11}$ (**2**) are isostructural and crystallize in the $R\bar{3}c$ space group with a natrotantite structure type. The compounds exhibit the 3D natrotantite structure in which α-U_3O_8-type sheets (P-layer) are connected by MnO_6 octahedra (O-layer). This is a novel framework topology for uranyl oxides. A^+ (A = K, Rb) cations reside in the void space between the MnO_6 octahedra (Figure 2). The layers repeat with the PO sequence commonly observed in the natrotantite structure type. The uranium atoms are in a 7-fold oxygen coordination environment, displaying a typical uranyl bonding motif of two short axial bonds and five longer equatorial bonds, one of which is weekly bound at 2.586(5)−2.604(5) Å. Table 2 lists the U−O bond distances for the title compounds. The UO_7 polyhedra share four of five equatorial edges with neighboring UO_7 polyhedra, forming a layer that has the same topology as α-U_3O_8. The U_3O_8-type layers are connected in the *c* direction by corner sharing of the uranyl oxygen atoms with MnO_6 octahedra. The Mn^{2+} cation positioned in a nearly regular octahedron exhibits Mn−O bond distances of 2.201(3)−2.208(4) Å.

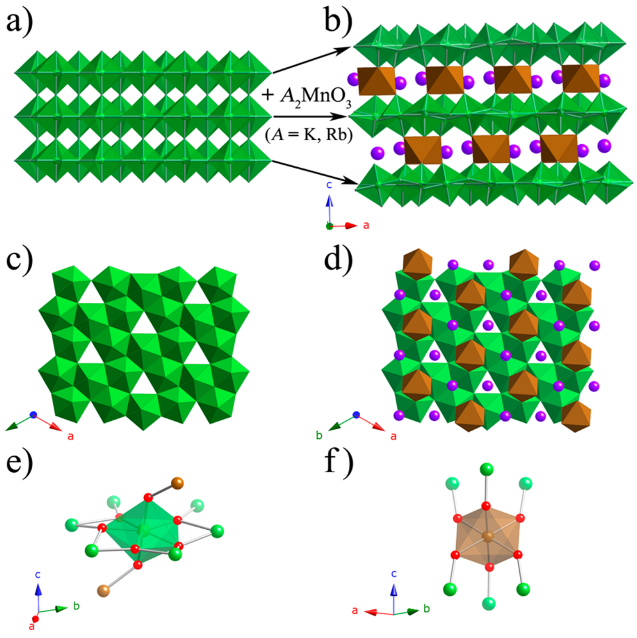

Figure 2. Uranyl sheet connectivities in α-U_3O_8 (a) and $K_2MnU_3O_{11}$ (**1**) (b), the top view of the uranyl sheet in **1** (c), the Mn/K layer on the uranyl sheet (d), the uranium environment in **1** (e), and the Mn environment in **1** (f). Potassium, manganese, uranium, and oxygen polyhedra/atoms are shown in violet, brown, green, and red, respectively.

Table 2. Selected Interatomic Distances (Å) for 1, 2, and 3

$K_2MnU_3O_{11}$			$Rb_2MnU_3O_{11}$		
U1	O1 × 2	1.902(4)	U1	O1 × 2	1.899(3)
	O2 × 2	2.2126(12)		O3 × 2	2.2164(11)
	O3 × 2	2.2151(11)		O2 × 2	2.232(5)
	O2	2.604(5)		O2	2.586(5)
$Li_{3.2}Mn_{1.8}U_6O_{22}$					
U1	O2	1.874(18)	U4	O18	1.846(17)
	O1	1.893(17)		O17	1.89(2)
	O7	2.16(2)		O7	2.202(19)
	O3	2.26(2)		O5	2.216(17)
	O5	2.28(2)		O15	2.31(2)
	O6	2.326(19)		O6	2.34(2)
	O4	2.38(2)		O16	2.42(2)
U2	O8	1.852(18)	U6	O21	1.83(2)
	O9	1.891(17)		O22	1.874(18)
	O12	2.17(3)		O12	2.18(3)
	O4	2.24(2)		O16	2.28(2)
	O11	2.29(2)		O10	2.292(19)
	O3	2.36(2)		O15	2.37(2)
	O10	2.40(2)		O11	2.49(2)
U3	O14	1.880(19)	U5	O20	1.862(18)
	O13	1.90(2)		O19	1.898(18)
	O15	2.19(2)		O3	2.16(2)
	O16	2.19(2)		O5	2.179(17)
	O6	2.203(19)		O4	2.19(2)
	O11	2.21(2)		O10	2.250(19)

DOI: 10.1021/acs.inorgchem.5b01004
Inorg. Chem. 2015, 54, 6993−6999

The Li compound, $Li_{3.2}Mn_{1.8}U_6O_{22}$ (**3**), is structurally related to the previous compounds exhibiting a 3D structure composed of uranium oxide sheets separated by lithium/manganese oxide sheets; however, the lithium ions are too small to be accommodated by the previous structure. The uranium oxide layers in this compound exhibit β-U_3O_8 topology. The difference between α- and β-U_3O_8 topologies is in the position of one oxygen atom, as illustrated in Figure 3, reducing the coordination of one of the uranyl environments from UO_7 to UO_6. In addition to β-U_3O_8,[62] there are four uranium-containing minerals that have exhibited this type of sheet topology, ianthinite,[63] billietite,[64] wyartite,[65] and spriggite,[66] where the interlayers are composed of H_2O molecules only, barium ions, calcium carbonate units, or lead/alkaline-earth atoms, respectively. The uranium atoms in **3** are found in 6- and 7-fold oxygen coordination environments (Figure 4), each with typical uranyl coordination with two short (1.83(2)−1.90(2) Å) and four (2.16(2)−2.250(19) Å) or five (2.16(2)−2.49(2) Å) long U−O bonds. The connecting layers are made up of four mixed Li/Mn sites with refined occupancies of Mn1/Li1 = 0.61(2)/0.39(2), Mn2/Li2 = 0.08(2)/0.92(2), Mn3/Li3 = 0.92(2)/0.08(2), and Mn4/Li4 = 0.22(2)/0.78(2) and one site occupied exclusively by Li that stack with a PO repeat sequence, using the previous convention. The disordered Mn/Li cations are observed in distorted octahedra with bond distances between 2.01(3) and 2.49(5) Å. The bond valence sums for the disordered Mn atoms, listed in Table 3, are +1.62−2.05. These sums are smaller than the valence of +2.65 obtained from charge balancing. Low bond valence sums have been observed in other Mn-containing oxides,[67] including structurally related $Cs_2Mn_3U_6O_{22}$,[68] and do not indicate that the composition is incorrect. The unique $Li(5)^+$ cation is found in an irregular LiO_5 polyhedron with Li−O bond distances of 2.03(5)−2.14(5) Å. All $(Mn/Li)O_6$ and LiO_5 polyhedra share their corners and edges with U−O layers along the *b* axis. The structure of the spriggite mineral, formally $(Pb_{2.77}Ca_{0.06}Ba_{0.04})$-$U_6O_{19.9}(OH)_2{\cdot}3H_2O$, represents the only previously reported 3D uranyl mineral composed of β-U_3O_8-type sheets, where the other reported minerals with this topology are 2D. The "Pb"-O interlayer of this structure has cavities and site mixing, much like **3**. A laboratory-grown compound, $[Ni(H_2O)_4]_3[U(OH,H_2O)(UO_2)_8O_{12}(OH)_3]$, synthesized under mild hydrothermal conditions, also has a 3D structure that consists of β-U_3O_8-type sheets connected by $NiO_2(H_2O)_4$ octahedra.[69] Unlike in the title compounds, where the Mn polyhedra are connected to multiple uranium polyhedra in each sheet, the Ni octahedra corner share with one uranium, through a uranyl oxygen, of each sheet, leading to a larger spacing between the β-U_3O_8-type sheets.

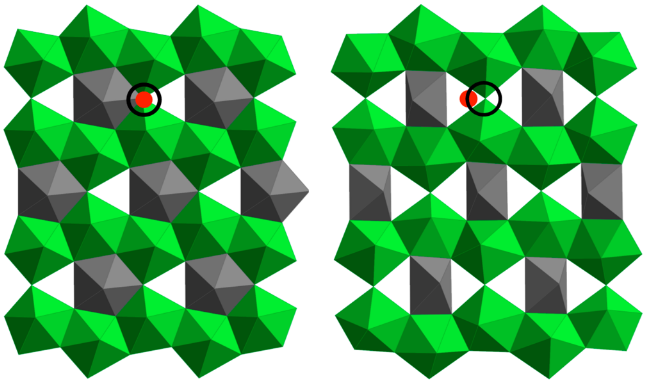

α-U_3O_8 Topology β-U_3O_8 Topology

Figure 3. Topology of α-U_3O_8 (left) and β-U_3O_8 (right). Uranium-oxide polyhedra are shown in green and gray, where the gray polyhedra are highlighting the topological change. The black circle shows the position of the oxygen atom that is responsible for the topological change, relative to its position in α-U_3O_8 (red dot).

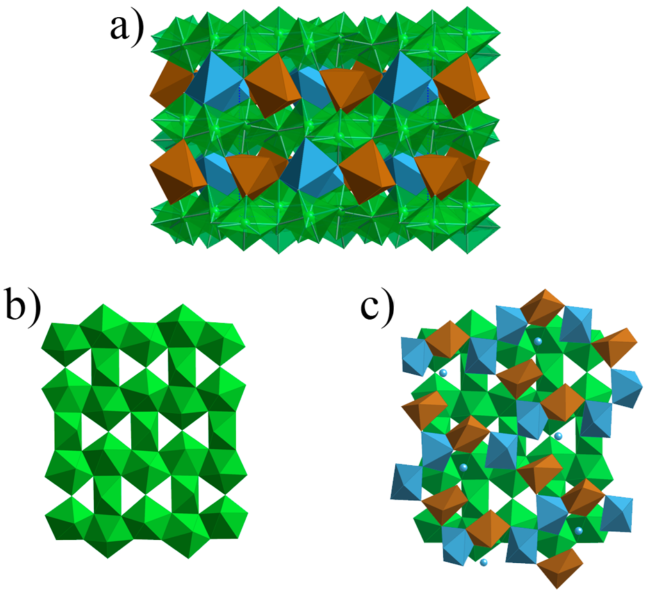

Figure 4. Uranyl sheet connectivities in $Li_{3.2}Mn_{1.8}U_6O_{22}$ (**3**) (a), the top view of the uranyl sheet (b), and the Mn/Li layer on the uranyl sheet (c). Lithium, manganese, and uranium polyhedra/atoms are shown in blue, brown, and green, respectively. The 100% Li site is represented by a sphere, and the mixed Li/Mn sites are presented as polyhedra with the color representing the predominant species.

Table 3. Bond Valence Sums for the Respective Atoms in 1, 2, and 3

$K_2MnU_3O_{11}$		$Rb_2MnU_3O_{11}$	
U1	5.93	U1	5.90
Mn1	1.94	Mn1	1.98
K1	1.11	Rb1	1.25
$Li_{3.2}Mn_{1.8}U_6O_{22}$			
U1	6.00	U4	5.99
U2	6.01	U5	5.82
U3	5.74	U6	5.96
Li1−Li4	0.68−0.85	Mn1−Mn4	1.62−2.05
Li5	0.98		

Although the reported compounds exhibit similar layered structures with the same PO stacking manner separated by A^+ and Mn cations, the structural families show two distinct U_3O_8-type topologies, α-type for **1** and **2** and β-type for **3**, shown in Figures 2c and 3b, respectively, and in more detail in Figure S3. It is thought that the size of the A^+ cations plays an important role in the formation of the different structures because **1** and **2** contain the large K^+ and Rb^+ cations, whereas **3** contains the much smaller Li^+ cation between the layers. This is clearly seen in the layer separation distances, e.g., one-sixth the *c* axes (6.1392 and 6.2587 Å) for **1** and **2** and half the *b* axis (5.4819 Å) for **3**, respectively. Figure 5 shows the environments surrounding the oxygens pertinent to the different sheet topologies for **1** and **3**. As shown by the translucent atoms, in

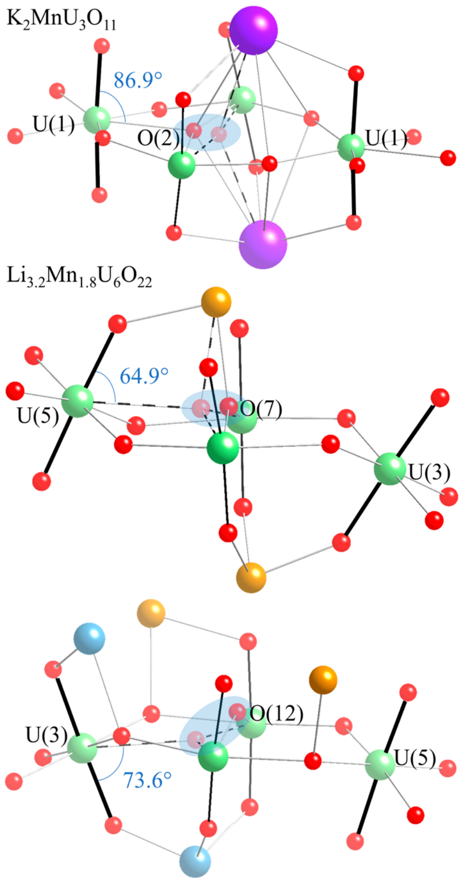

Figure 5. Environment surrounding the oxygen atoms pertinent to the different uranium sheet topologies in $K_2MnU_3O_{11}$ (top) and $Li_{3.2}Mn_{1.8}U_6O_{22}$ (bottom two). The uranyl bonds are shown in black, with the important uranyl bonds in bold. Potassium, lithium, manganese, uranium, and oxygen atoms are shown in purple, blue, brown, green, and red, respectively. The shaded area highlights the pertinent oxygen atoms, shown in solid red with solid bonds, and their location, if they adopted the other sheet topology, is shown in translucent red with striped bonds.

both compounds there is enough space for the oxygen atom to adopt either the α or β topology while maintaining the proper bond lengths with surrounding atoms. However, in $K_2MnU_3O_{11}$, the large, well-ordered K–Mn layers lead to the uranyl units to align closely with the stacking direction (uranyl *c*-axis angle = 80.3°). Furthermore, all of the U atoms within a layer are coplanar, as is observed in both α- and β-U_3O_8. As a result, the O═U–O(2) angle is 86.9°, close to the 90° expected in an ideal uranyl environment. On the other hand, in $Li_{3.2}Mn_{1.8}U_6O_{22}$, the smaller more disordered Li–Mn layers cause the uranyl units to tilt with respect to the stacking direction (uranyl *b*-axis angles = 63.8–76.8°). Furthermore, in order for the uranyl oxygens to bond with the smaller Li/Mn sites, the U atoms shift in the stacking direction and are no longer coplanar. As a result, if the pertinent oxygens were to adopt the α-type position, the O═U–O angles would be 64.9° [O(7)] and 73.6° [O(12)], respectively, far from the desired 90°. It is likely, for this reason, that the oxygens do not form this bond and therefore the β-U_3O_8 sheet topology is observed in **3**.

For **1** and **2**, there exist six A^+ and Mn^{2+} sites between the $U_6O_{22}{}^{8-}$ sheets if the formulas are doubled to $A_4Mn_2U_6O_{22}$, whereas for **3**, only five Li^+ and Mn sites are available due to the compact layer formation. The loss of a cation site in **3** is charge-compensated through Mn/Li site mixing and by the Mn atoms becoming mixed +2/+3 valent. Site mixing is favorable in the Li analogue due to the similar ionic size of Li^+ (0.76 Å) and Mn^{2+} (0.83 Å) for a 6-fold coordination environment. The site mixing does not occur in **1** and **2** due to the large ionic radii of the A^+ cation, 1.38 Å (K) and 1.52 Å (Rb), and since the A^+ and Mn^{2+} cations can occupy six crystallographic sites due to the large space between the layers.

The oxidation state of uranium for **1** and **2** should be carefully examined because they both exhibit relatively long U–O distances on equatorial positions that are also found in α-U_3O_8 having a mixed-valence of U^{5+} and U^{6+}. As listed in Table 3, the bond valence sum calculations using the optimized parameters provided by Burns,[70] r_{U-O} = 2.051 and b = 0.519 resulted in values of 5.90–5.93, which is in good agreement with uranium in the +6 oxidation state. The bond valences in α-U_3O_8, 5.27–5.40, are noticeably lower due to the presence of U^{5+}. Moreover, our magnetic measurements, discussed below, confirm the +6 valence state of uranium in our samples. Therefore, there is no doubt that the uranium atoms are in a hexavalent oxidation state, which is consistent with our synthetic method that is carried out in air and that uses extremely oxidizing, high-temperature conditions. Since the uranyl oxygen atoms are not shared with any other uranium centers in **1**, **2**, or **3** because of the layer separation by A^+ and Mn^{2+} cations, these materials exhibit Type **0** uranyl cation–cation interactions.[71]

Optical Spectroscopy. UV–vis diffuse reflectance data were measured on ground crystals of **1** and **2** and converted to absorbance vs wavelength plots using the Kubelka–Munk function.[72] Both compounds displayed a broad absorption band covering 200–700 nm (see Figure S4). With an estimated band gap of 1.44–1.58 eV, these materials can be classified as semiconductors.

Magnetic Property Measurement. The temperature dependence of the magnetic susceptibility measured in an applied field of 1000 Oe for **1** is shown in Figure 6. The susceptibility increases gradually with decreasing temperature and follows Curie–Weiss behavior throughout the entire temperature range. The inverse susceptibility data were fit to the Curie–Weiss law, $\chi = C/(T - \theta)$, where C is the Curie

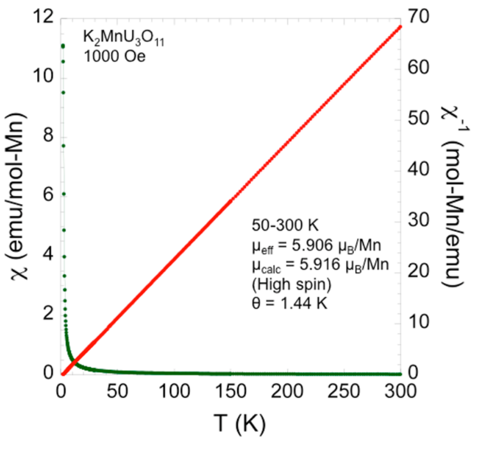

Figure 6. Temperature dependence of the magnetic susceptibility data (green) and the inverse susceptibility versus temperature plot with a fit to the Curie–Weiss law (red) for $K_2MnU_3O_{11}$ measured in an applied field of 1000 Oe.

constant and θ is the Weiss constant. On the basis of the linear fit, values of 4.36 emu·K·mol^{-1} and 1.44 K for C and θ, respectively, were extracted. From the Curie constant, the effective magnetic moment of 5.91μ_B for the Mn^{2+} cation was calculated, which is in excellent agreement with the theoretical value of 5.92μ_B calculated for the high-spin d^5 configuration of Mn^{2+}. The temperature dependence of the magnetic susceptibility for **2** is shown in Figure S5, where the same treatment was applied. The data showed no deviation from Curie−Weiss behavior. The observed magnetic moment, 5.78μ_B, deviates slightly from the expected value, 5.92μ_B, due to an approximate 4.4% impurity of a nonmagnetic, ternary Rb−U−O compound, with a likely composition of $Rb_2U_2O_7$, which can be seen in the PXRD plot (Figure S2).

■ CONCLUSIONS

The synthesis of three novel quaternary uranium oxides, $K_2MnU_3O_{11}$ (**1**), $Rb_2MnU_3O_{11}$ (**2**), and $Li_{3.2}Mn_{1.8}U_6O_{22}$ (**3**), was achieved by evaporation of a reactive chloride fluxes. **1** and **2** are the first examples of the natrotantite structure with UO_7 pentagonal bipyramidal, α-U_3O_8 topological sheets, whereas **3** has a related structure containing β-U_3O_8 topological sheets. The magnetic susceptibility data were collected for **1** and **2**; the compounds are paramagnetic throughout the collected temperature range, 2−300 K. The compounds also exhibit a broad absorption spanning 200−700 nm, with estimated band gaps of 1.44−1.58 eV.

■ ASSOCIATED CONTENT

Ⓢ Supporting Information

X-ray data in CIF format, powder XRD patterns, UV−vis spectra, magnetic susceptibility data, atomic coordinates and equivalent isotropic displacement parameters, and description of the structure solution on **3**. The Supporting Information is available free of charge on the ACS Publications website at DOI: 10.1021/acs.inorgchem.5b01004.

■ AUTHOR INFORMATION

Corresponding Author

*E-mail: zurLoye@mailbox.sc.edu. Phone: (803) 777-6916. Fax: (803) 777-8508.

Notes

The authors declare no competing financial interest.

■ ACKNOWLEDGMENTS

Research was supported by the U.S. Department of Energy, Office of Basic Energy Sciences, Materials Sciences and Engineering Division, under award DE-SC0008664.

■ REFERENCES

(1) Schleifer, M.; Busch, J.; Gruehn, R. *Z. Anorg. Allg. Chem.* **1999**, *625*, 1985−1990.

(2) Schleifer, M.; Busch, J.; Albert, B.; Gruehn, R. *Z. Anorg. Allg. Chem.* **2000**, *626*, 2299−2306.

(3) Busch, J.; Gruehn, R. *Z. Anorg. Allg. Chem.* **1996**, *622*, 640−648.

(4) Busch, J.; Hoffmann, G.; Gruehn, R. *Z. Anorg. Allg. Chem.* **1994**, *620*, 1056−1065.

(5) Busch, J.; Gruehn, R. *Z. Anorg. Allg. Chem.* **1994**, *620*, 1066−1072.

(6) Chen, C.-S.; Chiang, R.-K.; Kao, H.-M.; Lii, K.-H. *Inorg. Chem.* **2005**, *44*, 3914−3918.

(7) Lee, C. S.; Wang, S. L.; Lii, K. H. *J. Am. Chem. Soc.* **2009**, *131*, 15116−15117.

(8) Liu, H. K.; Chang, W. J.; Lii, K. H. *Inorg. Chem.* **2011**, *50*, 11773−11776.

(9) Liu, H. K.; Lii, K. H. *Inorg. Chem.* **2011**, *50*, 5870−5872.

(10) Chen, C. L.; Nguyen, Q. B.; Chen, C. S.; Lii, K. H. *Inorg. Chem.* **2012**, *51*, 7463−7465.

(11) Morrison, J. M.; Moore-Shay, L. J.; Burns, P. C. *Inorg. Chem.* **2011**, *50*, 2272−2277.

(12) Krivovichev, S. V.; Cahill, C. L.; Burns, P. C. *Inorg. Chem.* **2002**, *41*, 34−39.

(13) Siidra, O. I.; Nazarchuk, E. V.; Kayukov, R. A.; Bubnova, R. S.; Krivovichev, S. V. *Z. Anorg. Allg. Chem.* **2013**, *639*, 2302−2306.

(14) Locock, A. J.; Skanthakumar, S.; Burns, P. C.; Soderholm, L. *Chem. Mater.* **2004**, *16*, 1384−1390.

(15) Rivenet, M.; Vigier, N.; Roussel, P.; Abraham, F. *J. Solid State Chem.* **2007**, *180*, 713−724.

(16) Krivovichev, S. V.; Locock, A. J.; Burns, P. C. *Z. Kristallogr.* **2005**, *220*, 10−18.

(17) Krivovichev, S. V.; Burns, P. C. *Dokl. Phys.* **2004**, *49* (2), 76−77.

(18) Krivovichev, S. V.; Burns, P. C. *Solid State Sci.* **2003**, *5*, 373−381.

(19) Obbade, S.; Renard, C.; Abraham, F. *J. Solid State Chem.* **2009**, *182*, 413−420.

(20) Krivovichev, S. V.; Burns, P. C. *Inorg. Chem.* **2002**, *41*, 4108−4110.

(21) Bacmann, M.; Lambert-Andron, B. *Physica Status Solidi A* **1982**, *72*, 833−837.

(22) Surblé, S.; Obbade, S.; Saad, S.; Yagoubi, S.; Dion, C.; Abraham, F. *J. Solid State Chem.* **2006**, *179*, 3238−3251.

(23) Alekseev, E. V.; Krivovichev, S. V.; Depmeier, W.; Armbruster, T.; Katzke, H.; Suleimanov, E. V.; Chuprunov, E. V. *J. Solid State Chem.* **2006**, *179*, 2977−2987.

(24) Saad, S.; Obbade, S.; Yagoubi, S.; Renard, C.; Abraham, F. *J. Solid State Chem.* **2008**, *181*, 741−750.

(25) Duribreux, I.; Dion, C.; Abraham, F.; Saadi, M. *J. Solid State Chem.* **1999**, *146*, 258−265.

(26) Abraham, F.; Dion, C.; Saadi, M. *J. Mater. Chem.* **1993**, *3*, 459−463.

(27) Mer, A.; Obbade, S.; Rivenet, M.; Renard, C.; Abraham, F. *J. Solid State Chem.* **2012**, *185*, 180−186.

(28) Alekseev, E. V.; Krivovichev, S. V.; Depmeier, W. *J. Solid State Chem.* **2009**, *182*, 2977−2984.

(29) Obbade, S.; Dion, C.; Saadi, M.; Yagoubi, S.; Abraham, F. *J. Solid State Chem.* **2004**, *177*, 3909−3917.

(30) Obbade, S.; Dion, C.; Bekaert, E.; Yagoubi, S.; Saadi, M.; Abraham, F. *J. Solid State Chem.* **2003**, *172*, 305−318.

(31) Obbade, S.; Yagoubi, S.; Dion, C.; Saadi, M.; Abraham, F. *J. Solid State Chem.* **2003**, *174*, 19−31.

(32) Read, C. M.; Bugaris, D. E.; zur Loye, H.-C. *Solid State Sci.* **2013**, *17*, 40−45.

(33) Read, C. M.; Smith, M. D.; zur Loye, H.-C. *J. Chem. Crystallogr.* **2013**, *43*, 484−487.

(34) Roof, I. P.; Smith, M. D.; zur Loye, H.-C. *J. Cryst. Growth* **2010**, *312*, 1240−1243.

(35) Roof, I. P.; Smith, M. D.; zur Loye, H.-C. *Solid State Sci.* **2010**, *12*, 1941−1947.

(36) Roof, I. P.; Smith, M. D.; zur Loye, H.-C. *J. Chem. Crystallogr.* **2010**, *40*, 491−495.

(37) Bugaris, D. E.; zur Loye, H.-C. *Angew. Chem., Int. Ed.* **2012**, *51*, 3780−3811.

(38) Read, C. M.; Smith, M. D.; zur Loye, H.-C. *Solid State Sci.* **2014**, *37*, 136−143.

(39) Babo, J.-M.; Albrecht-Schmitt, T. E. *J. Solid State Chem.* **2013**, *197*, 186−190.

(40) Dion, C.; Obbade, S.; Raekelboom, E.; Abraham, F.; Saadi, M. *J. Solid State Chem.* **2000**, *155*, 342−353.

(41) Obbade, S.; Dion, C.; Duvieubourg, L.; Saadi, M.; Abraham, F. *J. Solid State Chem.* **2003**, *173*, 1−12.

(42) Read, C. M.; Smith, M. D.; zur Loye, H.-C. *J. Chem. Crystallogr.* **2014**, *44*, 604−608.

(43) Burns, P. C. *Can. Mineral.* **2005**, *43*, 1839−1894.
(44) Boltersdorf, J.; Wong, T.; Maggard, P. A. *ACS Catal.* **2013**, *3*, 2943−2953.
(45) Jahnberg, L.; Sundberg, M. *J. Solid State Chem.* **1992**, *100*, 212−219.
(46) McLamb, N.; Sahoo, P. P.; Fuoco, L.; Maggard, P. A. *Cryst. Growth Des.* **2013**, *13*, 2322−2326.
(47) Heunen, G. W. J. C.; IJdo, D. J. W.; Helmholdt, R. B. *Acta Crystallogr., Sect. C: Cryst. Struct. Commun.* **1995**, *51*, 1723−1725.
(48) Isobe, M.; Marumo, F.; Iwai, S.; Kimura, M. *Acta Crystallogr., Sect. B: Struct. Crystallogr. Cryst. Chem.* **1975**, *31*, 908−910.
(49) Putilin, S. N.; Krylov, E. A.; Men'shenina, N. F.; Evdokimov, A. A. *Zh. Neorg. Khim.* **1985**, *30*, 650−652.
(50) Hofmann, R.; Gruehn, R. *Z. Anorg. Allg. Chem.* **1991**, *602*, 105−117.
(51) Masó, N.; West, A. R. *J. Mater. Chem.* **2010**, *20*, 2082−2084.
(52) Palasyuk, O.; Maggard, P. A. *J. Solid State Chem.* **2012**, *191*, 263−270.
(53) Busch, J.; Hofmann, R.; Gruehn, R. *Z. Anorg. Allg. Chem.* **1996**, *622*, 67−75.
(54) *SMART, version 5.630, SAINT+, version 6.45, and SADABS, version 2.10*; Bruker Analytical X-ray Systems, Inc.: Madison, Wisconsin, 2003.
(55) Sheldrick, G. M. *Acta Crystallogr., Sect. A: Found. Crystallogr.* **2008**, *64*, 112−122.
(56) Hübschle, C. B.; Sheldrick, G. M.; Dittrich, B. *J. Appl. Crystallogr.* **2011**, *44*, 1281−1284.
(57) Parthe, E.; Gelato, L. M. *Acta Crystallogr., Sect. A: Found. Crystallogr.* **1984**, *40*, 169−183. Gelato, L. M.; Parthe, E. *J. Appl. Crystallogr.* **1987**, *20*, 139−143. Hu, S.-Z.; Parthe, E. *Chin. J. Struct. Chem.* **2004**, *23*, 1150−1160.
(58) (a) LePage, Y. *J. Appl. Crystallogr.* **1987**, *20*, 264−269. (b) Spek, A. L. *J. Appl. Crystallogr.* **1988**, *21*, 578−579. (c) Spek, A. L. *Acta Crystallogr., Sect. A: Found. Crystallogr.* **1990**, *46*, C34. (d) PLATON, A Multipurpose Crystallographic Tool, Utrecht University, Utrecht, The Netherlands, Spek, A. L., 1998.
(59) Morrison, G.; zur Loye, H.-C. *J. Solid State Chem.* **2015**, *221*, 334−337.
(60) Saine, M. C. *J. Less-Common Met.* **1989**, *154*, 361−365.
(61) Van Egmond, A. B. *J. Inorg. Nucl. Chem.* **1976**, *38*, 1649−1651.
(62) Loopstra, B. O. *Acta Crystallogr., Sect. B: Struct. Crystallogr. Cryst. Chem.* **1970**, *26*, 656−657.
(63) Burns, P. C.; Finch, R. J.; Hawthorne, F. C.; Miller, M. L.; Ewing, R. C. *J. Nucl. Mater.* **1997**, *249*, 199−206.
(64) Finch, R. J.; Burns, P. C.; Hawthorne, F. C.; Ewing, R. C. *Can. Mineral.* **2006**, *44*, 1197−1205.
(65) Hawthorne, F. C.; Finch, R. J.; Ewing, R. C. *Can. Mineral.* **2006**, *44*, 1379−1385.
(66) Brugger, J.; Krivovichev, S. V.; Berlepsch, P.; Meisser, N.; Ansermet, S.; Armbruster, T. *Am. Mineral.* **2004**, *89*, 339−347.
(67) Hannerz, H.; Svensson, G.; Esmaeilzadeh, S.; Grins, J. *Solid State Sci.* **1999**, *1*, 567−575.
(68) Read, C. M.; Gordon, E. E.; Smith, M. D.; Yeon, J.; Morrison, G.; Whangbo, M.-H.; zur Loye, H.-C. *Inorg. Chem.* **2015**, *54*, 5495−5503.
(69) Rivenet, M.; Vigier, N.; Roussel, P.; Abraham, F. *J. Solid State Chem.* **2009**, *182*, 905−912.
(70) Burns, P. C.; Ewing, R. C.; Hawthorne, F. C. *Can. Mineral.* **1997**, *35*, 1551−1570.
(71) Read, C. M.; Yeon, J.; Smith, M. D.; zur Loye, H.-C. *CrystEngComm* **2014**, *16*, 7259−7267.
(72) Kubelka, P.; Munk, F. *Z. Technol. Phys.* **1931**, *12*, 593−601.